

LETTER







## Identification of multiple eigenmode growth rates in DIII-D and EAST tokamak plasmas

To cite this article: Z.R. Wang *et al* 2019 *Nucl. Fusion* **59** 024001

View the [article online](#) for updates and enhancements.

## Letter

# Identification of multiple eigenmode growth rates in DIII-D and EAST tokamak plasmas

Z.R. Wang<sup>1</sup>, N.C. Logan<sup>1</sup>, S. Munaretto<sup>2</sup>, Y.Q. Liu<sup>2</sup>, Y.W. Sun<sup>3</sup>,  
S. Gu<sup>3</sup>, J.-K. Park<sup>1</sup>, J.M. Hanson<sup>4</sup>, Q.M. Hu<sup>1</sup>, T. Strait<sup>2</sup>, R. Nazikian<sup>1</sup>,  
E. Kolemen<sup>1</sup> and J.E. Menard<sup>1</sup>

<sup>1</sup> Princeton Plasma Physics Laboratory, Princeton, NJ 08543, United States of America

<sup>2</sup> General Atomics, PO Box 85608, San Diego, CA 92186-5608, United States of America

<sup>3</sup> Institute of Plasma Physics, Chinese Academy of Sciences, PO Box 1126, Hefei 230031, China

<sup>4</sup> Columbia University, 116th St and Broadway, New York, NY 10027, United States of America

E-mail: [zwang@pppl.gov](mailto:zwang@pppl.gov)

Received 14 October 2018, revised 22 November 2018

Accepted for publication 5 December 2018

Published 9 January 2019



CrossMark

## Abstract

The successful application of three-dimensional (3D) magnetohydrodynamic (MHD) spectroscopy in the stable DIII-D and EAST plasmas enables to directly extract the multi-mode plasma transfer function in tokamak experiments. The transfer function not only reveals the contribution of each dominant MHD eigenmode in the multi-mode plasma response, but also quantifies the corresponding eigenvalue which is the critical stability index of MHD mode. The method performs the active detection of stable plasma by utilizing the upper and lower rows of internal coils to scan the frequency and poloidal spectrum of the applied 3D field, and reconstructing the multi-mode transfer functions model through the least square fitting of the plasma response measured by 3D-field magnetic sensors distributed at different poloidal locations. The results point to the potential development of an advanced strategy for tracking the plasma stability based on the extracted eigenvalues of stable modes. The improved understanding of the dominant eigenmodes' behavior in multi-mode plasma response through transfer function can also help to optimize the applied 3D fields for the purposes, such as the type-I edge localized mode suppression and the core stability control in future fusion reactors.

Keywords: 3D MHD spectroscopy, transfer function, plasma response, plasma stability

(Some figures may appear in colour only in the online journal)

Tokamak plasmas often sensitively respond to a low level of intrinsically existing or externally applied non-axisymmetric (3D) magnetic field perturbations. The plasma response has been extensively investigated in experiments [1–5]. Since the perturbed field ( $\delta B$ ) is often several orders of magnitude smaller than the equilibrium field ( $B$ ), linear MHD theory is generally valid, and has therefore been extensively applied to understand the plasma response physics [6–10]. Much previous work [11–13] assumed that the plasma response is dominated by a single stable mode response. However, the combined response from multiple stable eigenmodes is

certainly a theoretical possibility, [14–21]. Crucially, measurements in DIII-D [22] have identified a multi-mode response in ITER similar shape RMP experiments.

Experiments also revealed that, at a given coil current, suppression of the type-I edge localized modes (ELMs) [23] depends on the poloidal spectrum of the applied vacuum RMP fields. The plasma response, which plays an important role in these ELM control experiments, sensitively depends on the applied perturbed field spectrum. The optimal poloidal spectrum for ELM control drives a large resonant response in the plasma edge [22, 24–26].

Generally, the response of the stable eigenmodes to the applied 3D field in experiments is still unclear, due to limited data measurements, particularly inside the plasma. Understanding the stability properties of these eigenmodes via plasma response measurements can be essential for (i) identification of the physics nature of the modes, e.g. the resistive wall mode [27] versus the tearing mode [28, 29]; and (ii) prediction and avoidance of severe disruptive events caused by these modes. The latter is particularly important for ITER [30], as well as for future high power fusion reactors.

The open loop transfer function [31] is a powerful tool to analyze the response and stability of a linear system. Here, the plasma response is denoted as total magnetic perturbations measured by the toroidally distributed 3D magnetic sensors, since the eigenmodes are the result of plasma interacting with vacuum vessel and other structures in tokamak system. Based on linear MHD theory and control theory, this work uses a new method for extracting multi-modal plasma response transfer functions from tokamak experiments. The extracted transfer functions reveal the contribution of each dominant eigenmode to the plasma response. This also allows us to quantify the damping rate of each stable mode individually, providing a critical assessment of the plasma stability. The method of obtaining the transfer function from the response to probing 3D fields is referred to as 3D MHD spectroscopy. In this work, we utilize the upper and lower rows of internal 3D magnetic coils equipped in DIII-D [4] and EAST [32], by scanning both the coil current phasing  $\Delta\phi = \phi_{\text{up}} - \phi_{\text{low}}$  and a finite (limited) range of the excitation frequency  $f$ . Here, the phasing ( $\Delta\phi$ ) is the difference between the upper row coil current phase ( $\phi_{\text{up}}$ ) and the lower row coil current phase ( $\phi_{\text{low}}$ ).

The measured magnetic response signals at multiple locations distributed poloidally along the tokamak vessel, can be represented by rational functions of the applied phasing and frequency (i.e. a Padé approximation). The poles and residuals of the rational functions reveal the stability properties as well as the response amplitudes of individual dominant eigenmodes simultaneously existing in the plasma. The method introduced here avoids the disadvantage of the conventional Nyquist analysis technique, which requires a wide range scan of  $f \in (-\infty, +\infty)$ , in order to accurately extract the transfer function. Such a scan, based on experimental measurements, is however not straightforward, since the wall eddy current shielding and/or contamination by other higher frequency MHD events can lead to the weak and noisy magnetic response in the high frequency range. The 3D MHD spectroscopy approach, introduced here, reduces the requirement of high frequency scans by including scans in another dimension: the poloidal spectrum of the applied field manipulated via  $\Delta\phi$ . This not only obtains more data points when  $f$  is not very high, but also make more changes to amplify different eigenmodes for cleaner magnetic measurements at different  $\Delta\phi$ . This choice is particularly reasonable when the wall eddy current response plays an important role in the total field response since the major variation of total response occurs when  $f$  is comparable to the inverse of the field penetration time through the wall, which is typically several milliseconds. Simultaneous fitting of the measured data in 2D parameter

space (frequency versus coil phasing) significantly improves the accuracy of the constructed transfer functions. This is the major advantage of the present approach.

When applying a rotating 3D field with toroidal number  $n$ , the measured plasma response  $\delta B$  on  $k$ th sensor can be approximated by the transfer function,

$$P_k(\Delta\phi, f) = \frac{\delta B}{I} = \sum_{j=1}^N \frac{u_k^j + l_k^j e^{-i\Delta\phi}}{if - \gamma_j} + u_{k\infty} + l_{k\infty} e^{-i\Delta\phi}. \quad (1)$$

Here,  $I$  is the amplitude of the rotating current in the 3D coils.  $\gamma_j$  is the eigenvalue of  $j$ th eigenmode and  $N$  is the total number of eigenmodes included in the transfer function. Note that each eigenmode shares the same eigenvalue at every sensor.  $u_k^j$  and  $l_k^j$ , as the upper and lower coil residuals (complex coupling coefficients), represent the local structure of  $j$ th eigenmode at  $k$ th sensor.  $u_{k\infty}$  and  $l_{k\infty}$ , which are similar to  $u_k^j$  and  $l_k^j$  defined with respect to the upper and lower coils, represent the local structure of residual response in vacuum at  $k$ th sensor when  $|f| \rightarrow \infty$  and other terms in equation (1) are vanished. In other words, these constant terms correspond to the finite magnetic response in the vacuum when the plasma and the resistive wall both become superconducting due to the fast rotating fields. Similar to [33], this formulation assuming the plasma response is the sum of contributions from multiple dominant eigenmodes can be derived from the discretized, linear, 3D MHD equations.

To extract the above multi-modal transfer function from DIII-D experiments, coil currents with frequencies  $f \in [-110 \text{ Hz}, -60 \text{ Hz}, -30 \text{ Hz}, -10 \text{ Hz}, 10 \text{ Hz}, 30 \text{ Hz}, 60 \text{ Hz}, 110 \text{ Hz}]$  were applied with phasings  $\Delta\phi \in [0 \text{ deg}, 60 \text{ deg}, 120 \text{ deg}, 180 \text{ deg}, 240 \text{ deg}, 300 \text{ deg}]$ , where the amplitude of coil current in upper ( $I_{\text{up}}$ ) and lower ( $I_{\text{low}}$ ) rows are the same and about 1kA,  $I_{\text{up}} = I_{\text{low}} \sim 1 \text{ kA}$  in the experiments. Each pair of  $(\Delta\phi, f)$  was applied in isolated time interval containing multiple periods to reduce the uncertainty in the response measurements. Six repeated shots (170200, 170202, 170203, 170204, 170205, 170220) were performed with the same plasma conditions to accomplish the scan, with each shot containing applied fields with a fixed phasing and a randomized frequency scan to remove any slowly evolving temporal bias from the frequency dependence. The magnetic response to the applied fields was measured by poloidal and radial field sensor arrays near the mid-plane of the low field side (LFS) and high field side (HFS) of the inner vessel wall. The names of four sensor arrays are MPID66M, ISLD, MPID1A, ISLD1A, respectively. The configuration of magnetic probes are described in [20, 34]. Each array contains multiple sensors distributed toroidally, enabling a fit to the amplitude and phase of the response in each toroidal mode number  $n = 1, 2, 3$ . Figure 1 shows one of the six discharges, where coil currents with  $\Delta\phi = 240^\circ$  are applied to generate  $n = 1$  3D perturbations in the flattop phase with almost constant plasma current ( $I_p$ ), safety factor ( $q_{95}$ ) and normalized beta  $\beta_N$ . In figure 1(b), the  $n = 1$  component of coil current, extracted from six toroidally distributed upper coil array, shows the sequence of different  $f$  applied in different

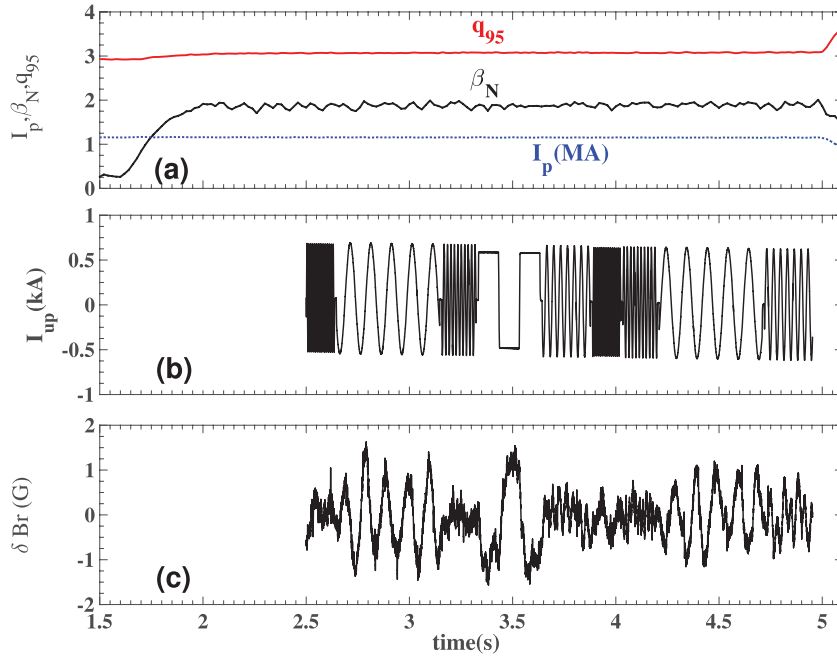


**Figure 1.** Time evolution of discharge 170220. The steady flattop  $I_p$ ,  $\beta_N$  and  $q_{95}$  are shown in (a). The wave form of applied current represented in (b) drives the  $n = 1$  magnetic response (c) measured by a radial sensor array located near the mid-plane of the HFS vessel wall.

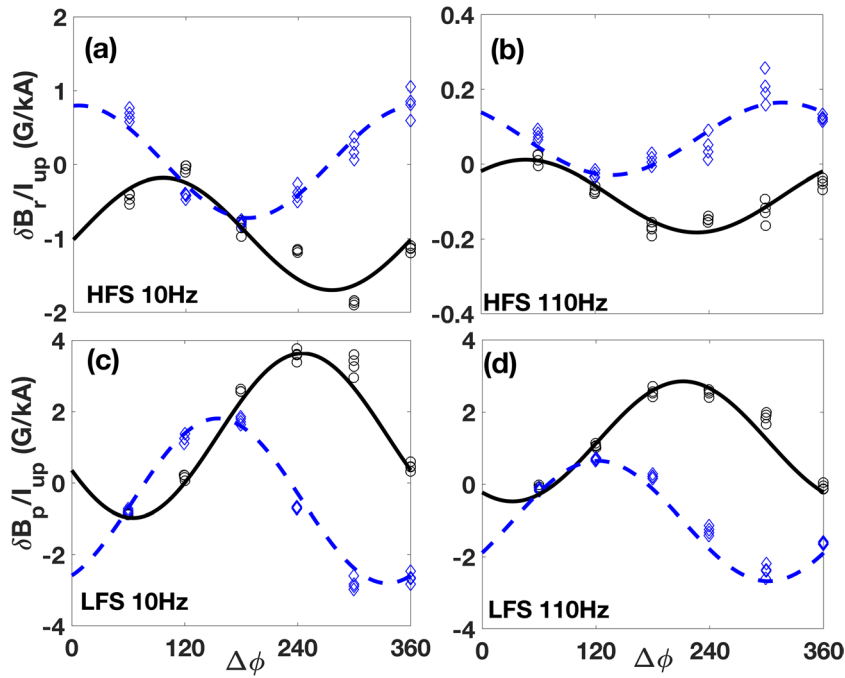


**Figure 2.** Coil current phasing comparison of magnetic response between experimental measurement ('o' real part and '◇' imaginary part) and the evaluation of transfer function ('solid line' real part and 'dashed line' imaginary part). The HFS radial field 10 Hz (a) and 110 Hz (b) response is shown as well as the LFS poloidal field 10 Hz (c) and 110 Hz (d) response.

time intervals. The  $n = 1$  magnetic response measured by the radial sensor array located near the middle plane of HFS (figure 1(c)) shows the associated variation in response amplitude. Then, the amplitude and phase of the  $n = 1$  magnetic response, normalized by  $I_{up}$ , is determined by least squares fitting of the waveform  $\delta B/I_{up} = Ae^{i(\omega + \phi_{res})}$  for each array of sensors within each distinct time interval for each combination of  $(\Delta\phi, f)$ . Here,  $A$  is the amplitude of magnetic response

measured by the sensor,  $\phi_{res}$  is the phase of response relative to the upper coil current and  $\omega = 2\pi f$ , Note that  $I = I_{up}$  in equation (1) and the full magnetic field, not the isolated plasma response [22], is used here.

In the DIII-D experiments, since the time interval for each applied  $(\Delta\phi, f)$  is known, four data points are extracted by using the whole time interval and three successive sub-intervals for the fitting of each  $(\Delta\phi, f)$  combination. Figure 2

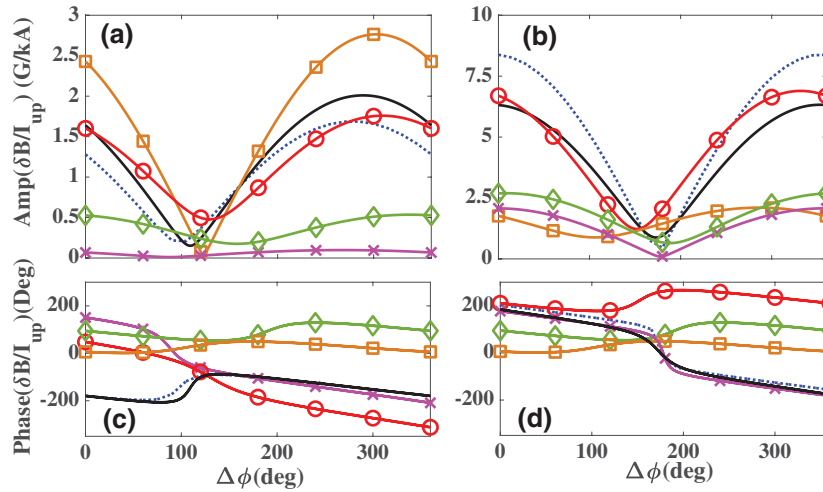


**Figure 3.** Phasing dependence of static magnetic response ( $f = 0$  Hz). (a, c) and (b, d) are the amplitude and phase of magnetic response measured by radial sensor located on the HFS (a, c) and LFS (b, d). The solid black line is the experimentally obtained transfer function. The curves marked by ‘□’, ‘o’ and ‘◇’ corresponding to 1st, 2nd and 3rd dominant modes of that transfer function respectively. Additionally, the curve marked by ‘x’ represents the constant term of transfer function in equation (1). The dashed blue line is the transfer function obtained from a synthetic experiment utilizing the MARS-F model to perform a phasing scan.

illustrates the coil phasing dependence of the rotating  $n = 1$  radial field response,  $\delta B_r$ , measured by an array of saddle loops just above the HFS midplane (the ISLD1A array) and the rotating  $n = 1$  poloidal field response,  $\delta B_p$ , measured by an array of magnetic probes at the LFS mid-plane (the MPID66M array) when  $f = 10$  Hz and 110 Hz. The measured responses show a clear sinusoidal phasing dependence. Similar fits were made using the other components (poloidal and radial) at each side of the machine (HFS and LFS) as well, and show a similar sinusoidal dependence.

A nonlinear least square method is used to extract the plasma transfer function by fitting equation (1) to every  $\delta \bar{B}_k^l$  simultaneously. Here  $\delta \bar{B}_k^l = \delta B_k^l / I_{up}^l$ .  $\delta B_k^l$  is the complex magnetic response measured at one of four aforementioned sensor arrays, when the coil current  $I_{up}^l$  is applied with  $l$ th combination of  $(\Delta \phi_l, f_l)$ .  $k$  is the index of ISLD1A, MPID1A, ISLD, MPID66M sensor arrays. The target function is  $\min_x F(x)$ , where,

$$F(x) = \sum_k^S \left| \frac{\delta \bar{B}_k^l - P_k(\Delta \phi_l, f_l)}{\delta \bar{B}_k^l} \right|^2, \quad (2)$$

$x = (u_k^l, l_k^l, u_{k\infty}, l_{k\infty}, \gamma_j)$  and  $S$  is the number of measured data points. The convergence of extracted transfer function is checked by perturbing the initial guess. The transfer function generally well follows the DIII-D experimental points and is able to reproduce the observed response at each sensor array and  $(\Delta \phi, f)$  with accuracy similar to that as illustrated in figure 2. To quantify the general fitting accuracy, the fitting error  $\sqrt{F(x)/S} = 0.29$  and the reduced  $\chi^2 = 16.51$  [36] are also evaluated. Three dominant eigenmodes with the eigenvalues,  $\gamma_{1st} = -13.58 - 3.68i$  Hz,  $\gamma_{2nd} = -31.82 - 7.42i$  Hz and  $\gamma_{3rd} = -44.2 - 28.86i$  Hz are extracted by the multiple mode transfer function fitting process. Including additional modes has a negligible contribution to the plasma response. Here, the real component of the eigenvalues is the ‘damping rate’ index

of mode stability and negative values imply stable (driven) modes. The nonlinear fitting process finds only stable modes, consistent with the stable plasmas observed in the experiments. The imaginary part of eigenvalue represents the natural mode rotation frequency. The first two modes are identified as slow-rotating or even quasi-static, while the third is rotating with a significantly higher frequency. It is important to note that this technique is able to fit mode frequencies higher than any frequency applied by the coils in the experiment.

Figure 3 shows a zero-frequency ( $f = 0$ ) subset of the DIII-D data comparable to responses shown in previous work [22]. Here, the number and relative contribution of dominant modes is now revealed by the experimentally extracted transfer function. The solid curve in figure 3 shows the phasing dependence of the  $f = 0$  plasma response evaluated by the multiple mode transfer function. The contribution of each dominant mode, corresponding to each term in equation (1), is also plotted. Figure 3 reports the least stable mode dominates the  $n = 1$  HFS radial sensor measurements. Meanwhile, 2nd mode is also significant at HFS. On the LFS sensors, however, the second least stable mode makes the largest contribution to the measured amplitude. The least stable and third modes are comparable to each other and have minor contributions to the total response on the LFS radial sensors. Interestingly, the constant term is also significant at LFS. Theoretically, it is known that the magnetic response with  $|f| \rightarrow \infty$  gets zero magnetic response and the maximum measurement on LFS mid-plane radial sensor, when  $\Delta \phi = 180$  deg and  $\Delta \phi = 0$  deg respectively. The constant term, extracted from the nonlinear least fitting, has no such constrain, but still agrees with the theoretical predication. In a sense, it indicates the reliability of experimentally extracted transfer function.

The multiple mode transfer function, extracted from the experiments, is a good target for the model validation and the exploration of MHD physics. The phasing and frequency dependencies of transfer function can be used to compare with

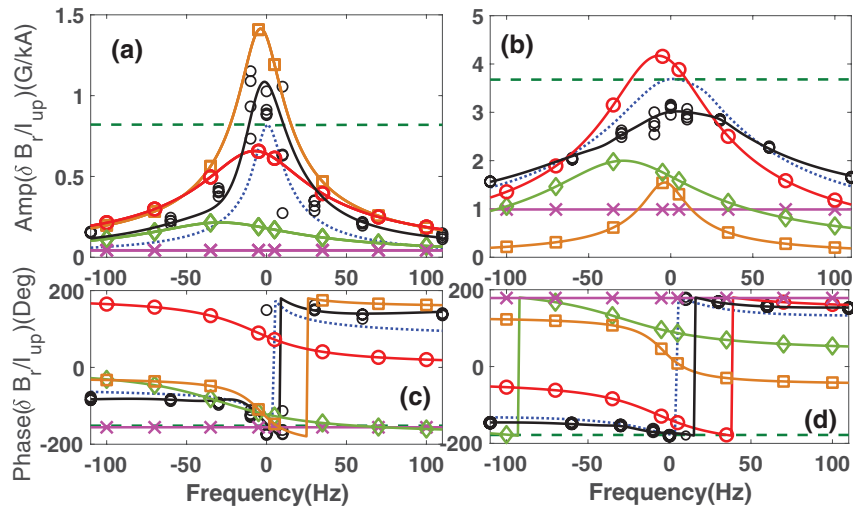


**Figure 4.** Frequency dependence of magnetic response. (a), (c) and (b), (d) are the amplitude and phase of magnetic response measured by radial sensor located at HFS and LFS. The experimental transfer function (black solid line) shows agreement with the experimental data points ('o') measured by 3D sensors. MARS-F simulation without wall (dashed line) and with wall (dotted line) is also compared here. The curves marked by '□', 'o', '◇' and 'x' correspond to 1st mode, 2nd mode, 3rd mode and the constant term of experimental transfer function respectively.

the simulated response directly. For instance, the linear ideal plasma response [6], simulated by MARS-F code [37, 38] generally shows agreement with the experimental transfer function in figure 3. The difference may be due to the equilibrium reconstruction and other detailed MHD physics, e.g. kinetic effects [9, 10]. Particularly, if the transfer function could be extracted from the numerical simulation, the mode response to 3D fields and the eigenvalue of each dominant mode can be compared between the experiments and simulations. The difference will help to make a detailed validation of the model and indicate if there is any essential or missed physics in the model.

The frequency dependent response measured in an independent discharge with the same equilibrium parameters is compared with the extracted transfer function in figure 4. The discharge only uses the upper coil to generate the rotating 3D fields. As expected by the linear response theory, setting  $I_k^j = 0$  and  $I_{k\infty} = 0$  in equation (1) yields a good agreement between the transfer function prediction and experimental radial field measurements. This is a comforting validation of the extracted transfer function and the linearity assumptions used therein. It also demonstrates the powerful ability to map predicted responses throughout the accessible coil frequency and phasing space using a relatively small number of discrete measurements.

The individual contributions of the three dominant modes are also presented in figure 4. The least stable mode dominates the peak HFS response and shows a significant frequency dependence due to the small amplitude of  $\gamma_{1st}$  which means the coil frequency can dominate in the denominator of least stable mode's transfer function. The second least stable mode, due to more stable  $\gamma_{2nd}$ , is much less sensitive to  $f$ . Since the multi-mode plasma transfer functions reveal the magnetic response of each dominant mode while applying different  $f$  and  $\Delta\phi$ , potentially, the transfer functions can help to find the optimal 3D fields which probably can better amplify the eigenmode related to the ELM suppression.

Ideal plasma response with/without 2D wall [9, 39], simulated by MARS-F code, is also presented in figure 4, where the wall model assumes the uniform resistivity and the wall time  $\sim 9$  ms which is typically used by MARS-F for  $n = 1$  DIII-D simulations [40]. The simulated plasma response is decreased as shown by the experimental transfer function while increasing  $f$ , since the eddy current in resistive wall plays an essential role in determining the magnetic response in the presence of rotating 3D fields. Meanwhile, the variation of simulated response with resistive wall is faster than that of experimental transfer function. While scanning the wall time in the simulation, no wall time can be found to make the variation of simulated response match the experimental transfer function for both radial LFS and HFS sensors simultaneously. As indicated in [40], the axisymmetric wall with uniform resistivity is not sufficient to resolve fine spatial details of wall eddy current patterns particularly to simulate the local magnetic measurements. The real DIII-D wall is complicated and requires more sophisticated wall modeling to make a reliable MHD simulation.

3D MHD spectroscopy is also validated in EAST experiments which utilize the upper and lower internal coils to scan  $\Delta\phi \in (0, 45, 90, 135, 180, 225, 270, 315)$  deg and  $f \in (-90, -60, -30, -10, 10, 30, 60, 90)$  Hz in five shots (70617, 70619, 70620, 70622 and 70633), where 1.3 kA coil current is applied to drive  $n = 1$  plasma response. Each shot scans two coil phasing with different frequencies. The experimental plasma is stable with almost constant  $\beta_N = 1.4$ ,  $I_p = 0.38$  MA and  $q_{95} = 4.7$  during the scan. In the EAST experiments, the transfer functions are extracted only at the radial and poloidal magnetic sensors located at the mid-plane of the LFS [35]. The HFS sensors are not used since the sensor arrays, installed behind the mechanical structure, and are thus well shielded from rotating fields. In the signal analysis of magnetic response, it is noted EAST magnetic sensors have higher measurement noise than DIII-D ones. Many factors, such as the

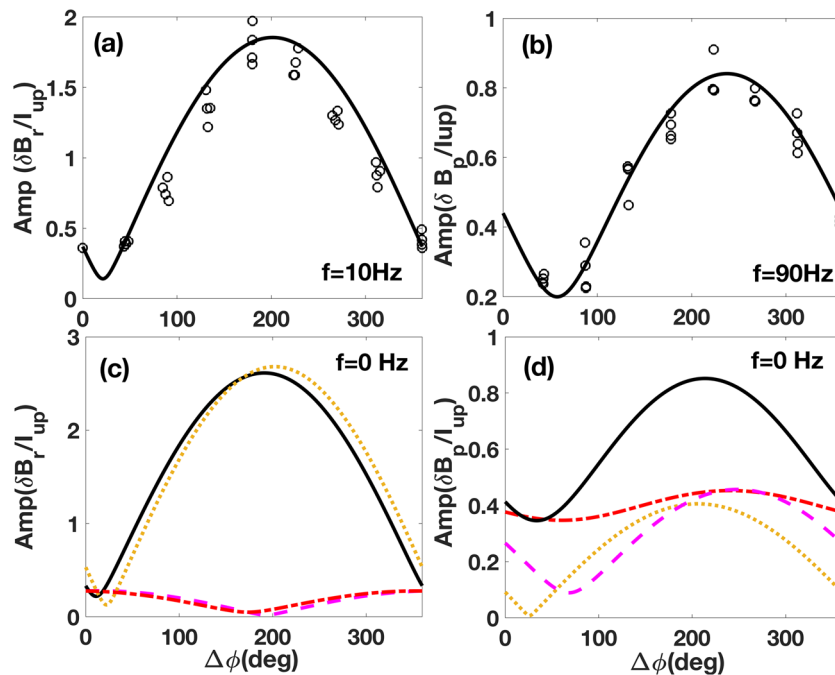


**Figure 5.** Coil phasing dependence of magnetic response. (a) and (b) illustrate the comparison between the experimental measurements ('o') and extracted transfer function (solid line) when  $f = 10$  Hz (a) and  $f = 90$  Hz (b). (c) and (d) present the contribution of 1st mode (dotted line), 2nd mode (dot-dashed line) and the constant term (dashed line) of transfer function (solid line) respectively, when the static 3D fields are applied. (a), (c) and (b), (d) are the amplitude of magnetic response measured by radial and poloidal sensors located at LFS respectively.

installation and calibration of sensors, can affect the response noise level and the accuracy of fitting process. However, the multi-mode transfer function still can be extracted with the comparable  $\sqrt{F(x)/S} = 0.33$  and  $\chi^2 = 20.56$  to DIII-D case. In general, the extracted transfer function well follows the behavior of measured response while varying  $\Delta\phi$  and  $f$ . Figures 5(a) and (b) illustrate the good correspondence between the transfer function and experimental measurements. Two dominant eigenmodes are extracted from the experimental measurements, with eigenvalues  $\gamma_{1st} = -10.61 - 0.01i$  Hz and  $\gamma_{2nd} = -146.3 + 17.23i$  Hz. Figures 5(c) and (d) show the relative contributions of each mode to the total response. In contrast to the DIII-D experiments, the least stable mode dominates the LFS radial magnetic response measurements in this EAST experiment. EAST results also show a much more stable secondary mode than DIII-D experiments.

In this work, 3D MHD spectroscopy, enabling to experimentally extracted the linear multi-mode plasma transfer function by fitting the magnetic response measured in the scan of 3D coil frequency and phasing, is successfully developed and applied in both DIII-D and EAST stable plasmas. The multi-mode transfer function shows the capability to quantify the number of dominant modes and the contribution of each mode in the multi-mode plasma response which is only qualitatively identified in previous work [22]. The plasma stability can be quantitatively inferred by the real parts of extracted eigenvalues in the transfer functions. Meanwhile, the imaginary parts of eigenvalues represent the natural mode rotation frequencies. Therefore, in the future experiments and numerical studies, the extracted modes' eigenvalues can help to understand the variation of stable modes' stability and rotation when the plasma

conditions, such as  $\beta$  and the plasma flow, are changed. Since the frequency and phasing response of each dominant mode can be interpreted by the extracted transfer functions, it has the potential to optimize the coil phasing and frequency to amplify the preferred eigenmode e.g. the edge peeling mode, to help ELM suppression. The efficiency of 3D MHD spectroscopy can also be greatly improved beyond this initial experimental proof of the concept. Employing  $n = 2$  3D MHD spectroscopy by applying wave packets of multiple coil frequencies and phasings can achieve a comparable scan to the one shown here for DIII-D in every 1.6 s of a discharge to extract the  $n = 2$  multi-mode plasma transfer function. In this DIII-D experiments, four phasings are scanned in four isolated time intervals. A wave packet, including multiple coil frequency, is applied in each interval and takes 400 ms to finish scan for each phasing. In principle, after first 1.6 s, the optimized 3D MHD spectroscopy allows to update the transfer function and report the plasma stability every 400 ms by using the new scanned phasing and the previous three ones. The analysis of this experiment is in progress and will be reported in the future paper. Further optimization of 3D MHD spectroscopy to achieve the real time detection of plasma stability can be important to predict and avoid MHD stabilities in ITER.

## Acknowledgments

This material is based upon work supported by the U.S. Department of Energy, Office of Science, Office of Fusion Energy Sciences, using the DIII-D National Fusion Facility, a DOE Office of Science user facility, under Awards DE-FC02-04ER54698 and DE-AC02-09CH11466. This work is also

supported by the National Natural Science Foundation of China under 11475224. DIII-D data shown in this paper can be obtained in digital format by following the links at footnote<sup>5</sup>. This manuscript has been authored by Princeton University under Contract Number DE-AC02-09CH11466 with the U.S. Department of Energy. The publisher, by accepting the article for publication acknowledges, that the United States Government retains a non-exclusive, paid-up, irrevocable, world-wide license to publish or reproduce the published form of this manuscript, or allow others to do so, for United States Government purposes.

## Disclaimer

This report was prepared as an account of work sponsored by an agency of the United States Government. Neither the United States Government nor any agency thereof, nor any of their employees, makes any warranty, express or implied, or assumes any legal liability or responsibility for the accuracy, completeness, or usefulness of any information, apparatus, product, or process disclosed, or represents that its use would not infringe privately owned rights. Reference herein to any specific commercial product, process, or service by trade name, trademark, manufacturer, or otherwise does not necessarily constitute or imply its endorsement, recommendation, or favoring by the United States Government or any agency thereof. The views and opinions of authors expressed herein do not necessarily state or reflect those of the United States Government or any agency thereof.

## ORCID iDs

Z.R. Wang  <https://orcid.org/0000-0002-7496-959X>  
 N.C. Logan  <https://orcid.org/0000-0002-3268-7359>  
 S. Munaretto  <https://orcid.org/0000-0003-1465-0971>  
 Y.W. Sun  <https://orcid.org/0000-0002-9934-1328>  
 S. Gu  <https://orcid.org/0000-0001-5159-939X>  
 J.E. Menard  <https://orcid.org/0000-0003-1292-3286>

<sup>5</sup> [https://fusion.gat.com/global/D3D\\_DMP](https://fusion.gat.com/global/D3D_DMP).

## References

- [1] Garofalo A.M. *et al* 1999 *Phys. Rev. Lett.* **82** 3811
- [2] Reimerdes H. *et al* 2004 *Phys. Rev. Lett.* **93** 135002
- [3] Reimerdes H. *et al* 2006 *Phys. Plasmas* **13** 056107
- [4] Lanctot M.L. *et al* 2010 *Phys. Plasmas* **17** 030701
- [5] Kirk A. *et al* 2013 *Nucl. Fusion* **53** 4
- [6] Park J.-K., Boozer A.H. and Glasser A.H. 2007 *Phys. Plasmas* **14** 052110
- [7] Liu Y.Q., Kirk A. and Nardon E. 2010 *Phys. Plasmas* **17** 122502
- [8] Boozer A.H. 2001 *Phys. Rev. Lett.* **86** 22
- [9] Wang Z.R. *et al* 2015 *Phys. Rev. Lett.* **114** 145005
- [10] Wang Z.R. *et al* 2018 *Nucl. Fusion* **58** 016015
- [11] Park J.-K. *et al* 2009 *Phys. Plasmas* **16** 082512
- [12] Garofalo A.M., Jensen T.H. and Strait E.J. 2003 *Phys. Plasmas* **10** 4776
- [13] Sabbagh S.A. *et al* 2013 *Nucl. Fusion* **53** 104007
- [14] Sabbagh S.A. *et al* 2006 *Phys. Rev. Lett.* **97** 045004
- [15] Sunn Pedersen T. *et al* 2007 *Nucl. Fusion* **47** 1293
- [16] In Y. *et al* 2008 *Phys. Plasmas* **15** 102506
- [17] Shiraki D. *et al* 2013 *Phys. Plasmas* **20** 102503
- [18] Logan N.C. *et al* 2018 *Nucl. Fusion* **58** 076016
- [19] King J.D. *et al* 2016 *Nucl. Fusion* **56** 014003
- [20] Munaretto S. *et al* 2018 *Phys. Plasmas* **25** 072509
- [21] Willensdorfer M. *et al* 2017 *Nucl. Fusion* **57** 116047
- [22] Paz-Soldan C. *et al* 2015 *Phys. Rev. Lett.* **114** 105001
- [23] Zohm H. 1996 *Plasma Phys. Control. Fusion* **38** 105–28
- [24] Liu Y.Q. *et al* 2011 *Nucl. Fusion* **51** 083002
- [25] Liu Y.Q. *et al* 1996 *Plasma Phys. Control. Fusion* **58** 11
- [26] Logan N.C. *et al* 2016 *Phys. Plasmas* **23** 056110
- [27] Liu Y.Q. and Bondeson A. 2000 *Phys. Rev. Lett.* **84** 5
- [28] Furth H.P., Killeen J. and Rosenbluth M.N. 1962 *Phys. Fluids* **5** 510
- [29] Glasser A.H., Greene J.M. and Johnson J.L. 1975 *Phys. Fluids* **18** 875
- [30] Ikeda K. 2007 *Nucl. Fusion* **47** S1
- [31] Girod B., Rabenstein R. and Stenger A. 2001 *Signals and Systems* 2nd edn (New York: Wiley) p 50
- [32] Sun Y. *et al* 2017 *Nucl. Fusion* **57** 036007
- [33] Liu Y.Q. *et al* 2004 *Nucl. Fusion* **44** 232
- [34] King J.D. *et al* 2014 *Rev. Sci. Instrum.* **85** 083503
- [35] Wang H.H. *et al* 2016 *Nucl. Fusion* **56** 066011
- [36] Wong M. 1997 *Computational Methods in Physics and Engineering* 2nd edn (Singapore: World Scientific) p 264
- [37] Liu Y.Q. *et al* 2008 *Phys. Plasmas* **15** 112503
- [38] Yang S.X. *et al* 2018 *Nucl. Fusion* **58** 046016
- [39] Liu Y.Q. *et al* 2010 *Phys. Plasmas* **17** 072510
- [40] Hanson J.M. *et al* 2016 *Nucl. Fusion* **56** 106022